A laminar kinetic energy model based on the Klebanoff-mode dynamics to predict bypass transition

Loic Jecker, Olivier Vermeersch, Hugues Deniau, E. Croner, G. Casalis

A laminar kinetic energy model based on the Klebanoff-mode dynamics to predict bypass transition

L. Jecker

Rue des Jeunes Bois, Châteaufort CS 80112, 78772 Magny-les-Hameaux, France

O. Vermeersch, H. Deniau

2 av. Edouard Belin, 31055 Toulouse, France

E. Croner

Rue des Jeunes Bois, Châteaufort CS 80112, 78772 Magny-les-Hameaux, France

G. Casalis

10 av. Edouard Belin, 31055 Toulouse, France

Abstract

This article will introduce a new bypass-transition model based on the Klebanoff-mode dynamics. The model is built on the Laminar Kinetic Energy (LKE) concept, in order to be used in a Reynolds-Averaged Navier-Stokes (RANS) formulation. A new formulation of the LKE will be presented – it is based on a transport equation which quantifies the Klebanoff-mode amplification and destabilisation. This equation is included in a $k-\omega$ turbulence model – as Walters & Cokljat [1] suggested – and is to result in a three-equation $k_L - k_T - \omega$ formulation. This new model was designed according to bypass-transition descriptions available in the literature. These descriptions are based on experimental results, Direct Numerical Simulation (DNS) results and stability computations. The bypass-transition phenomenon will first be overviewed and the mechanisms of the growth and the destabilisation of the Klebanoff modes will be examined.

Email address: Loic.Jecker@onera.fr (L. Jecker)
[1]Ph.D. Candidate, Safran Tech and ONERA, France
[2]Ph.D., ONERA DMPE
[3]Ph.D., Safran Tech
[4]Professor, form. ONERA and now Sc. Dep. Dir. of ISAE-SUPAERO

Starting from this literature review, a new model will then be described and validated on academic configurations.

Keywords: Laminar Kinetic Energy (LKE), bypass transition, Klebanoff modes

---

Nomenclature

d	Wall distance	m
k_L	Laminar kinetic energy (LKE)	$(\mathrm{m/s})^2$
k_T	Turbulent kinetic energy (TKE)	$(\mathrm{m/s})^2$
Re_L	Reynolds number based on the length L	
S_{ij}	Strain rate tensor, $S_{ij} = \frac{1}{2}\left(\frac{\partial U_i}{\partial x_j} + \frac{\partial U_j}{\partial x_i}\right)$	s^{-1}
S	S_{ij} magnitude, $S = \sqrt{2S_{ij}S_{ij}}$	s^{-1}
Tu	Turbulence intensity, $Tu = \sqrt{\frac{\sum_i u_i^2}{3U_e^2}}$	
(U_i)	Mean flow velocity (U, V, W)	m/s
(u_i)	Disturbance flow velocity (u, v, w)	m/s
ν	Kinematic viscosity	m^2/s
μ	Dynamic viscosity	kg/m/s
ρ	Density	$\mathrm{kg/m}^3$
ω	TKE specific dissipation	s^{-1}

Subscripts

i, j	Variable number
st	Streak-related
T	Turbulent-flow related
L	Laminar-flow related

Superscript

$'$	Turbulent values

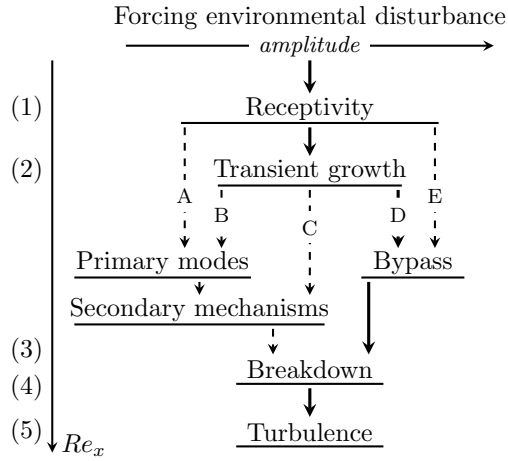

Figure 1: The routes to turbulence, according to Morkovin [2]. The numbering that was added refers to the bypass-transition scenario depicted in Fig. 2.

1. Context & Objectives

Laminar-to-turbulent transition is highly difficult to predict because it is still not totally understood nowadays. One can find various boundary-layer transition scenarios depending on multiple parameters which correspond to environmental disturbances. They can be roughly decomposed into the following steps: firstly a receptivity stage, secondly an instability amplification stage (that can possibly be decomposed in linear and non-linear stages), and finally the fully turbulent region. During the receptivity stage, free-stream disturbances are filtered and enter the boundary layer to generate new instabilities. Fig. 1 presents the possible routes to turbulence as a function of the environmental disturbances, as Morkovin *et al.* [2] explained.

Scenario A from Fig. 1 can be observed for the smallest free-stream turbulence (FST) levels and consists in the exponential growth of uncorrelated modes (modal instabilities), be they either Tollmien-Schlichting (TS) waves in a 2D flow, or crossflow modes in 3D flow (on a swept wing for instance). These disturbances are well-known and well-predicted by linear stability theories. Sta-

bility theories are commonly combined with other methods, such as the N-factor one – which was first developed by van Ingen [3] and Smith [4] in 1956 – in order to predict the location of the transition onset.

With a higher FST, Klebanoff modes – also called streaks because of their visual appearance – come out. Scenario B can be observed in the case of FST levels below $\sim 0.7\%$ and consists in the interaction between TS modes and Klebanoff modes.

Scenario C corresponds to a case where the free-stream turbulence level is high enough for the Klebanoff modes to totally overwhelm the modal instability. The optimal disturbance theory [5, 6, 7, 8] shows that the initial disturbances are streamwise vortices, leading to the formation of streamwise streaks. The transition is triggered by a secondary instability which grows in the mean flow, that is distorted by the propagation of Klebanoff modes.

In scenario D, the Klebanoff-mode dynamic entirely controls the boundary-layer transition. The high-frequency vortices entering the boundary layer are not filtered enough anymore and the interaction between these vortices and the streaks leads to the breakdown.

Scenario E takes place whenever the free-stream turbulence level is so high that a linear amplification cannot be observable anymore. The laminar state of the boundary layer is consequently limited or non-existent.

The *bypass transition* usually refers to any path that does not involve modal transition. However, it will be exclusively used here to refer to scenario C or D. This transition scenario has a key feature – the Klebanoff modes, whose amplification is well-predicted by the optimal disturbance theory.

The bypass transition can be observed on turbomachinery configurations, where the Reynolds numbers are moderate and the free-stream turbulence level is elevated. The Klebanoff modes are formed by the free-stream turbulence forcing on the laminar boundary layer and the resulting transition region potentially covers a large zone of the turbine or compressor blade (Mayle [9]). As a result, the prediction of the transition onset location is of significant importance to accurately compute the efficiency of the engine's components, which is a critical

parameter during the design process.

Data correlations were traditionally used to predict bypass transition in boundary-layer computations. The model developed by Abu-Ghannam and Shaw in 1980 [10] is the most popular one. Their formulation uses the momentum thickness and the turbulence level in a criterion to indicate the transition onset. However, the use of the momentum thickness makes this criterion difficult to use in realistic configurations, because, as Durbin [11] indicates, "it can be difficult if not impossible, to compute the momentum thickness on a complex geometry."

In order to predict bypass transition on complex geometries, RANS models were adapted in order to take this phenomenon into account. Three main approaches emerged [11]: firstly, the adaptation of a data-based correlation to RANS requirements (Menter *et al.* formulation for instance [12]); secondly, the fact of leaning on a turbulence model to simulate the transition [13, 14], or finally, the reliance on physical modelling. None of these approaches provided an accurate modelling until now. As Durbin pointed out in 2017 [11], "there is a need to improve predictive models."

In this article, the literature review that was used to write the model will first be presented. Both the process of bypass transition and existing laminar-kinetic energy models are exposed (section 2). In continuation, the model and its formulation will be introduced in three steps: firstly the Klebanoff-mode dynamic (their growth and destabilisation), secondly the turbulent boundary layer and finally the transition modelling (section 3). Results of the application of the new model on academic configurations will then be presented (section 4). Eventually, the predictive capability of the model will be discussed (section 5).

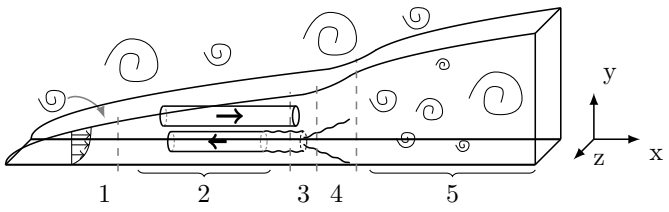

Figure 2: The bypass transition stages: 1) receptivity, 2) streak growth, 3) streak destabilisation, 4) turbulent spot birth and 5) turbulent boundary layer.

2. Literature review

2.1. Bypass transition

2.1.1. The bypass-transition process

The bypass transition is characterised by the birth of streamwise velocity fluctuations in the laminar boundary layer. These streaks-shaped velocity fluctuations are called Klebanoff modes. Their amplification and destabilisation are responsible for the bypass transition because their presence strongly modifies the stability properties of the boundary layer. It is Dryden who first observed these modes in 1937. Yet, Kline *et al.* [15] and Klebanoff [16] made a more complete description of their dynamic, respectively in 1967 and in 1971. Finally, Kendall [17] named these instabilities Klebanoff modes in 1985. The Klebanoff-mode growth was extensively and experimentally studied by Roach & Brieley [18], Westin *et al.* [19], Alfredsson & Matsubara [20, 21] and Jonáš *et al.* [22].

Although the streak growth can accurately be measured, the experimental evaluation of streak destabilisation can be considered difficult due to the spatial and temporal scales that are involved. The use of Direct Numerical Simulations (DNS) is therefore crucial to understand the bypass-transition dynamic, since they give an insight of the streak destabilisation mechanisms (Andersson *et al.* [23], Jacobs & Durbin [24], Brandt & de Lange [25] and Hack & Zaki [26]). Jacobs & Durbin showed in 2001 [24] that streaks are initiated by the penetration of low-frequency modes in the boundary layer. They constructed a turbulent inflow using Orr-Sommerfeld continuous modes and showed that non-

linear mechanisms generate the production of low-frequency modes. According to their analysis, the characteristics of the streaks generated inside the boundary layer (in terms of frequency contents) do not depend on the properties of the free-stream turbulence. Streaks are thus an "implicit property of the boundary layer" (Jacobs & Durbin [24]).

Another recent field of research encompasses the competition between streak and TS-waves. In 2017, Moore [27] confirmed Jacobs & Durbin's assertion that streaks are an implicit property of the boundary layer, also for small turbulence intensity level. She explained that, even with a leading-edge turbulence level of 0.042%, low-frequency modes grow linearly before the TS-waves lead to the boundary-layer destabilisation. For moderated free-stream turbulence level of $1-2\%$, Bose *et al.* showed in 2016 [28] that the combination of streaks and TS-waves gives birth to helical structures leading to the boundary-layer destabilisation.

The bypass-transition scenario is illustrated in Fig. 2 and decomposed into five steps:

1. **Receptivity**: vortices from the free-stream turbulence penetrate the laminar boundary layer. This receptivity phase is characterised by a high-frequency filtering, called the *shear-sheltering* and described by Jacobs & Durbin [24].
2. **Streak formation and growth**: these vortices interact with the boundary-layer shear to form the streaks. This mechanism is called the *lift-up* mechanism, explained by Landahl [29] and illustrated in Fig. 3. The lift-up mechanism consists in a mean-flow momentum displacement caused by the wall-normal part of the FST: the higher velocities from the upper part of the boundary layer move towards the wall while the lower velocities rise to the boundary-layer edge. This process leads to the creation of two types of streaks – *i.e.* "low-speed" streaks and "high-speed" streaks.
   Savill [30] explained this mechanism using the Reynolds-stress transport equation. The wall-normal turbulent velocity is denoted by v' and the

streamwise streak velocity by u_{st}. First, the kinetic energy of the wall-normal velocity fluctuation $\overline{v'^2}$ is transferred to the $\overline{u_{st}v'}$ correlation due to the boundary-layer shear. The $\overline{u_{st}v'}$ term combined with the boundary-layer shear then leads to a production of streamwise velocity fluctuation $\overline{u_{st}^2}$. The Klebanoff modes consequently formed are mainly composed of streamwise fluctuation energy.

They undergo then *transient growth*, an amplification process well-described by the optimal disturbance theory (ODT) [5, 6, 7, 8], which will be presented further in this article.

3. **Streak destabilisation**: the streak is destabilised whenever it reaches a significant amplitude – approximately $25-30\%$ of the mean-flow velocity [23]. Three breakdown scenarios could be identified with the help of DNS [23, 24, 26]:
   (a) Kelvin-Helmholtz instabilities: because of the streaks, two inflection points are formed. This causes a Kelvin-Helmholtz instability [23]. The first one comes from the superimposition of the mean boundary-layer velocity and the streak velocity. It appears in the upper region of the boundary layer, in wall-normal direction. The second one comes from the shear between two streaks of opposite direction, in spanwise direction [25].
   (b) TS-like waves: mainly when the pressure gradient is adverse, it is possible for TS-like waves to grow in the mean flow modified by the streaks and to destabilise the boundary layer [26].
   (c) FST penetration: a low velocity streak amplifies and rises in the boundary layer. When close to the boundary layer edge, it interacts with the FST, which can cause the formation of a turbulent spot inside the boundary layer, as Jacobs & Durbin [24] explained. Using DNS results, they showed that this scenario happens if the streak is of "sufficient amplitude" and located in the outer portion of the boundary layer.
4. **Turbulent spot birth**: the unstable streaks breakdown and form tur-

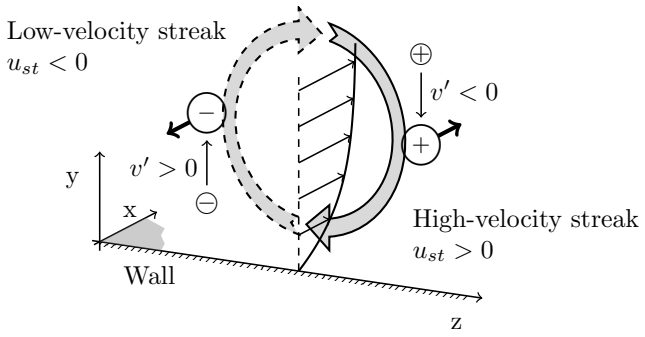

Figure 3: The lift-up mechanism in a boundary layer. The momentum is transported by the wall-normal free-stream turbulence v', to create streaks (low-speed and high-speed) inside the boundary layer.

bulent spots, which may either grow or disappear. Zaki [31] performed a statistical analysis of the turbulent-spot growth on DNS of streak destabilisation, showing that the volume of each spot evolves as a function of time, independently of the free-stream pressure gradient.

5. **Turbulent boundary layer**: the turbulent spots occupy the whole boundary layer, the turbulent state of the flow is generalized.

Durbin wrote in 2017 [11] that "the boundary layer response to forcing has an ubiquitous feature: the streaks." A good understanding of the streak dynamic seems to be essential to predict accurately both the transition onset and the transition length.

2.1.2. Klebanoff-mode amplification

The streak formation is attributed to the lift-up mechanism (cf. section 2.1.1). It consists in an energy transfer from the wall-normal FST $\overline{v'^2}$, filtered by the shear, to $\overline{u_{st}v'}$, and then to the streak $\overline{u_{st}^2}$. A key part of the streak modelling rests therefore on the representation of the filtered FST $\overline{v'^2}$ and on its impact on the $\overline{u_{st}^2}$ production.

Several authors identified the importance of $\overline{v'^2}$ in the bypass-transition prediction. Voke & Yang performed a large-eddy simulation (LES) of bypass transition

in 1995 [32]. They demonstrated that the interaction between the wall-normal turbulence and the mean shear leads to streak production. In 1997, Volino [33] suggested the following $-\overline{uv}$ stress model:

$$-\overline{uv} = A{v_e}'\delta_{99}\left(\frac{y}{\delta_{99}}\right)^b \frac{\partial U}{\partial y}, \tag{1}$$

with $A = 0.41$ and $b = 2.5$ two constants, δ_{99} the boundary-layer thickness and ${v_e}'$ the wall-normal FST. He compared this modelling to a standard mixing length model and showed better transition prediction ability for cases with FST level higher than 1%. These results also indicate that v' plays a significant role in boundary-layer transition submitted to high FST.

A different approach – explained by Andersson *et al.* in 1999 [5] and by Luchini in 2000 [6] – consists in calculating the disturbance that leads, in the case of a given base flow, to the greatest fluctuation-energy amplification. This approach is called the optimal disturbance theory (ODT) and relies on an optimisation problem which is itself based on the linearised Navier-Stokes equations. This method shows that, for a boundary-layer configuration, the optimal disturbance is initially wall-normal-oriented and leads to an amplification of the streamwise fluctuations. It is thus fully coherent with the lift-up mechanism. Another result is that the streamwise-induced disturbances are one order of magnitude in $\sqrt{Re_x}$ stronger than the velocity fluctuations in the other directions.

Biau *et al.* in 2007 [34] and Vermeersch *et al.* in 2010 [35] also used the linearised Navier-Stokes equations to predict bypass transition. Their work consists in solving the equation for the streamwise disturbance u_{st} with a modelling of the v' disturbance. A criterion is then applied to detect the streak destabilisation and to activate a turbulence model. The model of Vermeersch *et al.* is able to reproduce accurately the Klebanoff-mode growth on the tested cases.

2.2. Laminar kinetic energy models

The main idea for the Laminar Kinetic Energy (LKE) modelling is to add one transport equation for the variable k_L to a classic two-equation turbulence

model. This additional variable represents the energy of the velocity disturbances growing in the laminar boundary layer. This approach was introduced in 1997 by Mayle & Schulz [36], who wrote a new equation for k_L. However, the Mayle & Schulz formulation presents a key drawback: the production term of the LKE equation is based on pressure fluctuations, and LES results from Lardeau *et al.* [37] showed that this phenomenon is a source of energy dissipation for the streaks.

Walters & Leylek developed in 2004 [38] a LKE formulation based on the Boussinesq hypothesis for both turbulent and laminar velocity fluctuations. They defined two different eddy viscosities, separating the "large" coherent eddies from the small turbulent scales. This formulation is based on the $k-\epsilon$ turbulence model. In 2008, Walters & Cokljat [1] adapted the 2004 formulation for the $k-\omega$ turbulence model, which gave interesting results on the ERCOFTAC T3 cases [18].

The accurate representation of the role played by the FST wall-normal component in the production of laminar fluctuations is one of the main difficulties encountered with these formulations. In 2006, Sveningsson [39] proposed a solution implying the adaptation of the Walters & Leylek formulation with two additional equations issued from a v^2-f model. However, the author concluded that "the new model inherited the sensitivity to the free-stream length scale of the Walters & Leylek model." He thus suggested to revise the scale splitting used in the Walters & Leylek model. The various approaches highlight, as Lopez & Walters [40] indicated in 2015, that until today "there is no precise definition for LKE in the research community."

The present authors believe that an accurate bypass transition modelling cannot be written without taking the streak dynamic into account. It is for this reason that they chose to write a "physics-based" model. On the one hand, the equation for u_{st} developed by Vermeersch *et al.* reproduces accurately the Klebanoff-mode growth in the laminar boundary layer. It is however not directly usable in a RANS model. On the other hand, the LKE models take into account the existence of velocity fluctuations in the laminar boundary layer in a RANS

formulations. Nevertheless, none of these RANS formulations is based on an accurate description of the streak amplification. The model suggested in this article is consequently based on the LKE concept with a new definition of the variable k_L.

3. Formulation of a new model

As it was argued in section 2.1.1, the streaks constitute the key element of bypass-transition. It was thus chosen to model the kinetic energy of the streaks through the LKE k_L. The main innovation of the new model is a physics-based equation for k_L and the way it is taken into account in the Reynolds tensor. This modelling will be presented in subsection 3.1. The streak destabilisation will be studied in subsection 3.2. We will in particular study the way the transition onset is determined, as well as the way the transition extent is controlled. The full model will eventually be formulated in subsection 3.3.

3.1. Klebanoff-mode amplification modelling

3.1.1. Definition of the LKE

The velocity is decomposed into three parts: a mean flow component U_i and two fluctuation components – the turbulent one being u_i' and the streak-related one being $u_{st,i}$. The LKE represents the Klebanoff-mode energy in the laminar zone. Since these velocity fluctuations are predominant in the streamwise direction, the LKE k_L can be defined as the average energy of the streamwise velocity fluctuation associated to the local amplitude of the streak u_{st}:

$$k_L = \frac{\overline{u_{st}^2}}{2}. \tag{2}$$

A fundamental hypothesis has been formulated at this point. Although it is known that the streaks are not only streamwise-oriented, the wall-normal and the spanwise velocity fluctuations – which corresponds to a rotation of the streaks around the streamwise axis – will be neglected. Results of optimal disturbances theory calculations show that the streak velocity vector has an

order of magnitude of $\left(U_e,\ O\left(U_e/\sqrt{Re_x}\right),\ O\left(U_e/\sqrt{Re_x}\right)\right)$ [35]. The influence of the two non-streamwise components on the mean flow is thus negligible. The streak velocity vector is consequently reduced to $(u_{st},\ 0,\ 0)$. The definition of k_L induces a loss of knowledge on several streak properties. There is indeed no distinction between low-speed and high-speed streaks. Moreover, the spanwise wavelength information is lost as a mean amplitude of the streaks is calculated.

3.1.2. Equation for the Klebanoff-mode amplification

The streamwise velocity fluctuations in the laminar zone satisfy the Navier-Stokes equations:

$$\frac{\partial u'}{\partial t} + U_i\frac{\partial u'}{\partial x_i} + u'_i\frac{\partial U}{\partial x_i} + u'_i\frac{\partial u'}{\partial x_i} = -\frac{\partial p'}{\partial x} + \nu\frac{\partial^2 u'}{\partial x_i^2}. \tag{3}$$

Orders of magnitude are analysed with the help of Prandtl length scales: a reference scale L is used in the chordwise direction and a boundary-layer length scale $\delta = LRe_L^{-1/2}$ is used in the wall-normal and spanwise directions. The continuity equation for the mean flow and for the disturbances implies that V, W, v' and w' are scaled with $U_e/\sqrt{Re_L}$. The pressure perturbation is scaled with $\rho_e U_e^2/Re_L$.

The quadratic term in Eq. 3 is neglected to obtain a linear equation, which gives for a 2D mean flow:

$$\frac{\partial u'}{\partial t} + U\frac{\partial u'}{\partial x} + V\frac{\partial u'}{\partial y} + u'\frac{\partial U}{\partial x} + v'\frac{\partial U}{\partial y} = \nu\left(\frac{\partial^2 u'}{\partial x_i^2}\right). \tag{4}$$

From now on, it will be assumed that the turbulent streamwise fluctuation u' is neglected in the laminar boundary layer compared to the streak velocity u_{st}.

The equation is finally multiplied by u_{st} and averaged (in the Reynolds-average sense), which results in the following equation:

$$\frac{Dk_L}{Dt} = \underbrace{-\overline{u_{st}v'}\frac{\partial U}{\partial y}}_{P_{k_L}} \underbrace{-2\nu\left(\frac{\partial\sqrt{k_L}}{\partial x_i}\right)^2}_{D_{k_L}} + \underbrace{\nu\frac{\partial^2 k_L}{\partial x_i^2}}_{\Delta_{k_L}}. \tag{5}$$

The right-hand side of this transport equation can be decomposed into three separated terms:

- a production term P_{k_L}, which represents the lift-up effect through the multiplication of the $\overline{u_{st}v'}$ correlation by the shear of the mean flow;
- a viscous dissipation D_{k_L};
- a viscous diffusion Δ_{k_L}.

However, the $\overline{u_{st}v'}$ term is not known and requires modelling.

Results of optimal disturbances theory calculations showed that the correlation between u_{st} and v' is perfect and negative, because a positive v' produces low-velocity streaks ($u_{st} < 0$). As a consequence:

$$-\overline{u_{st}v'} = \sqrt{\overline{u_{st}^2}}\sqrt{\overline{v'^2}}. \tag{6}$$

Although the physical perturbation is however not optimal, measurements of bypass transition process on the ERCOFTAC T3 cases [18] indicate that the correlation $-\overline{u_{st}v'}/\sqrt{\overline{u_{st}^2}.\overline{v'^2}}$ is approximately constant in the boundary layer. As the FST is modelled by the turbulent kinetic energy (TKE) k_T, $\overline{v'^2}$ is considered to be proportional to k_T. Finally, $\overline{u_{st}v'}$ is written as follows:

$$-\overline{u_{st}v'} = \alpha\sqrt{k_L k_T}. \tag{7}$$

The coefficient α contains the correlation between u_{st} and v' and the proportionality between $\overline{v'^2}$ and k_T. In order to reproduce the measurements from ERCOFTAC cases, this coefficient is set to $\alpha = 0.063$.

3.1.3. Influence of Klebanoff modes on the mean flow

The influence of the velocity fluctuations on the mean flow is modelled by the Reynolds-stress tensor $\overline{u_i u_j}$. The decomposition of the velocity fluctuations in two parts (the Klebanoff-mode part $u_{i,st}$ and the turbulent part u_i') leads to a three-term Reynolds stress:

$$\begin{aligned}\overline{u_i u_j} &= \overline{\left(u_i' + u_{i,st}\right)\left(u_j' + u_{j,st}\right)} \\ &= \underbrace{\overline{u_i' u_j'}}_{\text{(a)}} + \underbrace{\overline{u_{i,st}u_{j,st}}}_{\text{(b)}} + \underbrace{\overline{u_i' u_{j,st}} + \overline{u_{i,st}u_j'}}_{\text{(c)}}.\end{aligned} \tag{8}$$

This Reynolds stress is decomposed into:

- the classic turbulent stress given by the turbulent model (a);
- a streak part representing the influence of Klebanoff modes on the mean flow (b);
- the coupling between both (c).

As the streak is modelled as a pure streamwise fluctuation, the streak-related tensor $\overline{u_{i,st}u_{j,st}}$ has a single non-zero component, $\overline{u_{st}^2} = 2k_L$. This tensor is thus synonymous of a monodimensional turbulence tensor. It was also assumed that only the wall-normal part of the turbulence interacts with the streaks, the only non-zero component of the interaction tensor is therefore the $\overline{u_{st}v'}$ term (and its symmetric). The whole Reynolds-stress tensor consequently takes the following anisotropic form in the boundary-layer:

$$\overline{u_i u_j} = \overline{u_i' u_j'} + \begin{pmatrix} 2k_L & -\alpha\sqrt{k_L k_T} & 0 \\ -\alpha\sqrt{k_L k_T} & 0 & 0 \\ 0 & 0 & 0 \end{pmatrix}. \tag{9}$$

The $\overline{u_i' u_j'}$ tensor is given by the turbulent model.

3.2. Klebanoff-mode destabilisation modelling

3.2.1. Detection of the transition onset

From a statistical point of view, and as discussed in section 2.1.1, DNS results show that the bypass-transition triggering always occurs in the case of a significant streak amplitude [26]. The proposed criterion consequently puts in comparison the streak amplitude k_L and the local shear:

$$\frac{k_L}{\nu \frac{\partial U}{\partial y}} > C_{onset}, \tag{10}$$

with $C_{onset} = 11$. Figure 4 shows a graphical representation of the criterion, calculated with the current model for three ERCOFTAC T3 cases. The threshold value of the criterion is reached when a curve crosses the dotted line; the vertical lines mark the measured transition location. The criterion proposed in Eq. 10 is consistent with the scenario that Jacobs & Durbin described in 2001

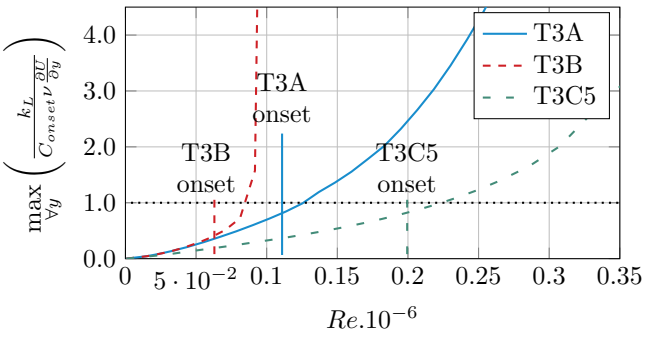

Figure 4: Transition-onset criterion calculated for the ERCOFTAC T3A (a), T3B (b) and T3C5 (c) cases.

[24]. According to their analysis, a streak has to fulfil two criteria in order to be destabilised: on the one hand, it has to be of "sufficient amplitude" – corresponding to a significant k_L -; on the other hand, it has to be located in the outer portion of the boundary layer – corresponding to a sufficiently low shear.

Once the transition criterion is verified, k_L tends towards zero because the Klebanoff modes vanish in the turbulent boundary layer. The criterion proposed in Eq. 10 is thus not verified after the transition onset. In other words, the knowledge that the transition onset was reached is lost. This criterion is consequently modified in order to be verified in the turbulent boundary layer as well:

$$\frac{k_L + 3k_T}{\nu\frac{\partial U}{\partial y}} > C_{onset}. \tag{11}$$

The coefficient multiplying k_T does not change the results for most of the tested cases, as k_L is at least ten times greater than k_T near the transition onset. However, a coefficient around 3 shows better results when the turbulence level Tu is higher than 5%.

3.2.2. Transition-onset information propagation

In the equations of the model, several terms depend on the flow regime. Once the criterion from Eq. (10) is verified, the laminar terms are replaced by their turbulent formulation. Nevertheless, the criterion will never be verified

in the whole boundary layer, that is to say, in a small region near the wall $k_T < \frac{C_{onset}}{3}\nu\frac{\partial U}{\partial y}$. The Walters & Cokljat model shows a similar behaviour. k_L continues to exist in the turbulent boundary layer, in a thin region near the wall. Since k_L was defined as the streak kinetic energy, and since the streaks vanish in the turbulent boundary layer, the choice was made to make P_{k_L} disappear in the fully turbulent zone flow so that k_L tends towards zero. Once the criterion is verified, the information has to propagate everywhere in the boundary layer downstream to cause the change of regime from laminar to turbulent effective.

It was thus suggested to transport a transition indicator β, that equals zero in the laminar boundary layer and grows once the criterion is satisfied:

$$\frac{D\rho\beta}{Dt} = \rho P_\beta, \tag{12}$$

with the production term P_β written as follows (σ_β being a model's constant):

$$P_\beta = \sigma_\beta f_{crit}\,(1-\beta)\,S, \tag{13}$$

$$f_{crit} = \begin{cases} 1 & \text{if} \quad \frac{k_L+3k_T}{\nu\frac{\partial U}{\partial y}} > C_{crit}, \\ 0 & \text{otherwise.} \end{cases} \tag{14}$$

The equation for β is written so that β grows along streamlines, but will not propagate in other directions. The transition function f_{tr} is thus based on the maximum of β, searched in the wall-normal direction:

$$f_{tr} = \max_{\forall d}(\beta)\,. \tag{15}$$

This function consequently grows in the transition region. It will be used to control the transition dynamic. A turbulent indicator β_{BP} is defined, it equals 0 in the laminar boundary layer and 1 once the transition has begun. It is defined as:

$$\beta_{BP} = 1 - \exp(-100 f_{tr})\,. \tag{16}$$

While f_{tr} is used to control the transition gradually, the role of β_{BP} is to change abruptly once the transition criterion is verified.

3.3. Full formulation of the model

The turbulent modelling rests on an adaptation of the k_T and ω equations from the Walters & Cokljat formulation. The full four-equation $k_L - k_T - \omega - \beta$ formulation is summarised here:

$$\begin{array}{rcl}
\frac{D(\rho k_L)}{Dt} & = & \rho P_{k_L} - \rho T_k - 2\mu \left(\frac{\partial \sqrt{k_L}}{\partial x_j}\right)^2 + \frac{\partial}{\partial x_j}\left[\mu \frac{\partial k_L}{\partial x_j}\right], \\
\frac{D(\rho k_T)}{Dt} & = & \rho P_{k_T} + \rho T_k - \rho \omega k_T - 2\mu \left(\frac{\partial \sqrt{k_T}}{\partial x_j}\right)^2 \\
 & & + \frac{\partial}{\partial x_j}\left[\left(\mu + \frac{\rho \alpha_T}{\sigma_k}\right)\frac{\partial k_T}{\partial x_j}\right], \\
\frac{D(\rho \omega)}{Dt} & = & C_{\omega,1}\frac{\rho\omega}{k_T} P_{k_T} + \rho\left(\frac{C_{\omega,R}}{f_W} - 1\right)\frac{\omega}{k_T} T_k - \rho C_{\omega,2} f_W^2 \omega^2 \\
 & & + \frac{\partial}{\partial x_j}\left[\left(\mu + \frac{\rho \alpha_T}{\sigma_\omega}\right)\frac{\partial \omega}{\partial x_j}\right], \\
\frac{D(\rho \beta)}{Dt} & = & \rho \sigma_\beta f_{crit}\,(1-\beta)\,S,
\end{array} \tag{17}$$

The boundary conditions at the wall are:

- $k_L = k_T = 0$;
- $\frac{\partial \omega}{\partial y} = 0$.

The Reynolds stress inside the boundary-layer is formulated:

$$\overline{u_i u_j} = \overline{u_i' u_j'} + \begin{pmatrix} 2k_L & -\alpha\sqrt{k_L k_T} & 0 \\ -\alpha\sqrt{k_L k_T} & 0 & 0 \\ 0 & 0 & 0 \end{pmatrix}. \tag{18}$$

The turbulent stress is formulated with the Boussinesq hypothesis:

$$\overline{u_i' u_j'} = \frac{2}{3} k_T \delta_{ij} - 2\nu_T S_{ij}, \tag{19}$$

with the following eddy viscosity:

$$\nu_T = f_\nu C_\mu f_W^2 \frac{k_T}{\omega}. \tag{20}$$

The f_ν, C_μ and f_W functions come from the Walters & Cokljat model [1]. The viscous wall effect is accounted for by the viscous damping function f_ν (A_ν is constant):

$$f_\nu = 1 - \exp\left(-\frac{f_W\sqrt{R_T}}{A_\nu}\right), \quad R_T = \frac{k_T}{\nu\omega}. \tag{21}$$

The turbulent viscosity coefficient C_μ is written as proposed by Shih *et al.* [41] to satisfy the realisability constraint (A_0 and A_S are constant):

$$C_\mu = \frac{1}{A_0 + A_S S\omega^{-1}}. \tag{22}$$

The kinematic wall effect is incorporated in f_W by comparing the effective turbulent length scale λ_{eff} to the wall distance d (C_λ is constant):

$$\lambda_{eff} = \min\left(C_\lambda d, \lambda_T\right), \quad \lambda_T = \frac{\sqrt{k_T}}{\omega}, \tag{23}$$

$$f_W = \left(\frac{\lambda_{eff}}{\lambda_T}\right)^{\frac{2}{3}}. \tag{24}$$

The k_L production term is written as:

$$P_{k_L} = \left[(1-\beta_{BP}) + \beta_{BP}\max\left(0, 1-1.1f_{tr}\right)\right]\alpha\sqrt{k_L k_T}S, \tag{25}$$

so that it disappears in the turbulent region. The k_T production is written as:

$$P_{k_T} = (1-\beta_{BP})\,k_T\omega + \beta_{BP} f_{tr} f_\nu C_\mu f_p^2 \frac{k_T}{\omega} S^2, \tag{26}$$

therefore k_T does not grow in the laminar boundary layer, where $\beta_{BP} = 0$. The use of f_p instead of f_w is justified by the TKE amplification dynamic in the transition region:

$$\begin{gathered} f_p = \max\left(f_W, 1 - 0.7\exp\left(-\sqrt{\frac{Re_y}{37}}\right)\right), \\ \text{with } Re_y = \frac{y\sqrt{k_T}}{\nu}. \end{gathered} \tag{27}$$

Once the transition has begun, turbulent spots appear and spread out in the boundary layer, fuelled by the energy of the streaks. Physically, kinetic energy is transferred from the coherent low-frequency velocity fluctuations (streaks) to the higher frequencies of the turbulence, until the streaks vanish completely. The transition dynamic is therefore controlled by three terms in the model – on the one hand, a transfer term T_k, to discharge energy from k_L to k_T during the transition process; on the other hand, the k_T and k_L production terms. The

$C_{\mu,std} = 0.09$	$C_{\omega,1} = 0.44$
$C_\lambda = 2.495$	$C_{\omega,2} = 0.92$
$A_\nu = 6.75$	$C_{\omega,R} = 1.5$
$\sigma_k = 1.0$	$\sigma_\omega = 1.17$
$A_0 = 4.04$	$A_S = 2.12$

$\alpha = 0.063$	$C_{onset} = 11.0$
$C_T = 1.5 \times 10^{-2}$	$\sigma_\beta = 1.3 \times 10^{-2}$

Table 1: The constants for the turbulent region (from WC [1]) are displayed on the superior table. The constants for the laminar and transition regions are displayed on the inferior table.

transfer term T_k is proportional to k_L divided by a time. The characteristic time is related to the boundary-layer state, through its shear S:

$$T_k = f_{tr} C_T k_L S. \tag{28}$$

The model constants are gathered in Table 1. Fig. 5 provides a summary of the bypass-transition scenario and how the new model represents each step. The graph below the boundary-layer sketch displays the evolution of f_{tr} and β_{BP} along the longitudinal axis.

In the new model, the following points finally differ from the Walters & Cokljat formulation:

- a new equation is presented for k_L, based on the physics of Klebanoff-mode;
- a new criterion for transition onset is written;
- a new Reynolds stress has been formulated taking the streak anisotropy into account;
- the k_T production term is modified in the laminar zone so that k_T does not grow as long as the transition criterion has not been verified;

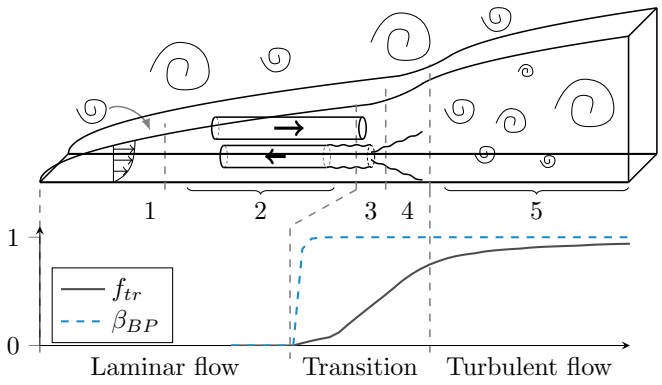

Figure 5: The bypass-transition stages and how the model represents them through f_{tr} and β_{BP}.

- a new transport equation is proposed for β and is used for the transition dynamic control;
- the transfer term is rewritten;
- the production damping of k_L – in the turbulent region – and the k_T production damping – in the laminar zone – are both done with β;
- the turbulent production P_{k_T} is modified in the laminar and the transition regions. Since the f_{INT} function is not useful anymore, it is therefore not used;
- the new k_L equation does not rest on the scale separation suggested by Walters & Cokljat. The f_{SS} and $f_{\tau,l}$ functions are consequently not kept;
- the $P_{\omega,3}$ term bends the velocity profile, as exposed in Appendix A. It is useful as far as the behaviour of $f_{\tau,l}$ is concerned. Since the function $f_{\tau,l}$ is not used anymore, the $P_{\omega,3}$ term is removed from the equation for ω;
- the near-wall dissipation of k_T includes a factor 2, following the result obtained with asymptotic developments (Jones *et al.* [42]).

4. Application on academic configurations

The numerical results presented in this article are provided by the new model integrated in a boundary-layer code – 3C3D. The numerical parameters used to run the following test cases can be found in Appendix B, in Tab. B.2 and B.3.

4.1. Influence of the turbulence intensity on bypass transition

The FST level plays a major role in the bypass transition since it corresponds to the streaks' source of energy through the lift-up mechanism. The ERCOFTAC T3 [18] zero-pressure-gradient cases – T3A and T3B – were used to validate its influence in the new model. Figure 6 represents the streamwise evolution of the maximum velocity-fluctuation along the wall-distance normalised by the free-stream velocity U_e for the ERCOFTAC T3A and T3B cases. The streamwise velocity fluctuations calculated by the model is composed of the streak velocity $u_{st} = \sqrt{2k_L}$ and the turbulent velocity u'. Three zones appear:

- The laminar zone, where only the streak velocity-fluctuation grows. The streak amplification is well-predicted by the model on both cases.
- The transition zone, where the u' value grows and reaches its turbulent level while u_{st} decreases.
- The turbulent zone, where the laminar fluctuations decay to become negligible compared to the turbulent ones.

Three markers (**(i)**, **(ii)** and **(iii)**) highlight the three key steps of the modelling:

- Label **(i)** corresponds to the transition onset, where the k_L and k_T behaviour must be controlled in order to ensure the continuity of the Reynolds stress. If this process is not accomplished properly, a short return to the laminar state could be noticed on the skin friction C_f and the shape factor H_{12} before reaching their turbulent values;
- Label **(ii)** corresponds to the end of the transition region, which, according to the experimental data, is not abrupt and can only be kept smooth by the calculation if k_L is not dissipated too early.

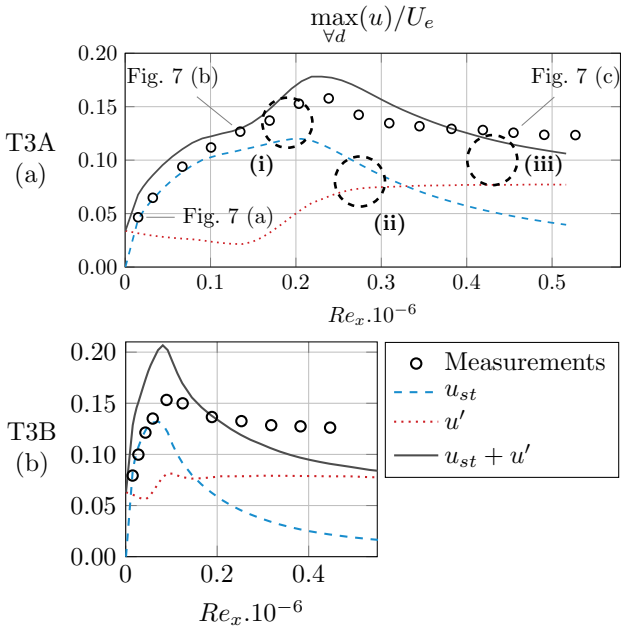

Figure 6: Maximum amplitude of the streamwise velocity-fluctuation, divided by the local free-stream velocity U_e for the ERCOFTAC T3A (a) and T3B (b) cases [18] (symbols). The dashed line corresponds to the streak fluctuation, the dotted line to the turbulent fluctuation and the plain line to the total velocity fluctuation.

- Label **(iii)** corresponds to the fully turbulent flow, where the computations do not match the measurements. The calculated turbulence underpredicts the u' level. This discrepancy is attributed to the use of the Boussinesq hypothesis, which does not enable to calculate accurately the anisotropy of the velocity fluctuations in a boundary-layer flow.

To evaluate the modelling of the Klebanoff-mode dynamics by the LKE, Fig. 7 depicts the velocity-fluctuation profiles along the wall-normal direction at three streamwise stations. The streak fluctuation (dashed lines), the turbulent fluctuation (dotted lines) and the total fluctuation (plain lines) are drawn separately in the figure. In the laminar zone (a and b) the fluctuation-velocity profile calculated by the optimal disturbance theory (ODT) and normalised by the wall-normal maximum of u_{st} is added to the figure (dashed-dotted line). At the first station (a), both the ODT and the new model predict accurately the position of the wall-normal maximum of the streamwise fluctuation-velocity. The turbulent profile u' shows that k_T is dissipated by the shear in the laminar boundary layer. It reaches the measured streamwise velocity fluctuation outside the boundary layer. However, the sum of u_{st} and u' overpredicts the measured total velocity fluctuation. This is also visible in Fig. 6, in which the plain line is situated higher than the measurements in the laminar zone. This difference is attributed to the modelling of the turbulence in the laminar boundary layer. The turbulence behaviour in a laminar boundary layer is not well-known and the classical two-equation turbulence model – from which the k_T and ω equations result – are not developed for laminar boundary layers. Since the u' profile does not correspond to a physical turbulent velocity profile in this region, the α coefficient in equation (7) was written so that the streak velocity maximum matches the measured velocity fluctuation maximum. For this reason, in Fig. 6, it is the dashed line – the calculated streak fluctuation – that crosses the symbols – the measured fluctuation – in the laminar zone, not the plain line.

At the second station (b), the maximum of the measured streamwise fluctuation-velocity shifts towards the wall. This trend is not captured by the ODT. The

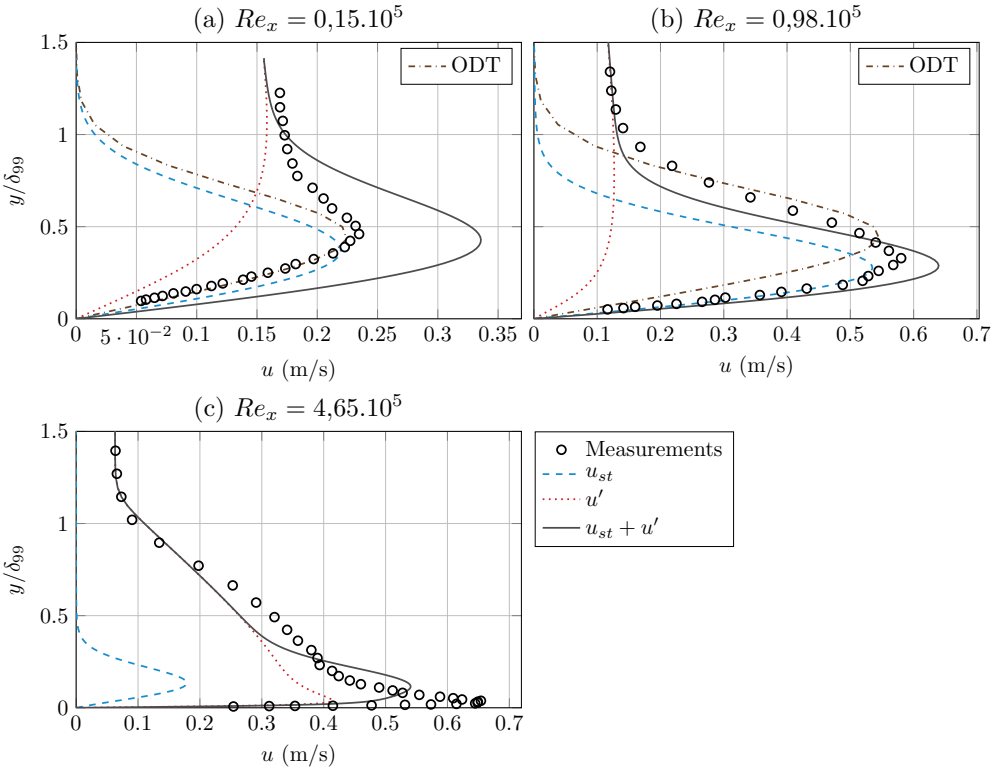

Figure 7: Velocity-fluctuation profiles in the wall-normal direction for three x-stations of the T3A case (symbols). The dashed line corresponds to the streak fluctuation, the dotted line to the turbulent fluctuation, the plain line to the total velocity fluctuation and the dashed-dotted line to ODT results (in frame (a) and (b) only).

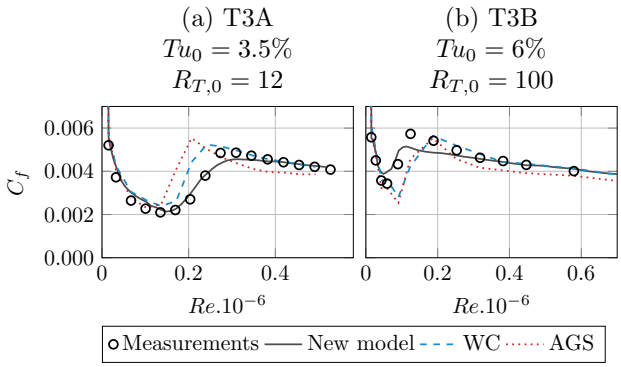

Figure 8: Skin friction coefficient for the ERCOFTAC T3A (a) and T3B (b) cases (symbols), calculated with the new model (plain line), the Walters & Cokljat model (WC, dashed line) and the Abu-Ghannam and Shaw criterion (AGS, dotted line).

new model predicts a streak profile u_{st} moving closer to the wall, the predicted total fluctuation $u_{st} + u'$ then reproduces the measured profile pretty well. The location of the total velocity fluctuation is once again well predicted. Moreover, since the predicted turbulent velocity becomes negligible compared to the predicted streak velocity, the difference between the predicted total fluctuation velocity and the measured one decreases.

At the last station (c), situated in the fully turbulent boundary layer, k_L is decaying to zero. The velocity-fluctuation profile is thus mainly controlled by k_T. The calculated turbulent profile finely predicts the shape of the measured one, but the amplitude of u' is underestimated. This difference is also visible in Fig. 6 and is attributed to the Boussinesq hypothesis, as indicated above.

Fig. 8 shows the streamwise evolution of the skin friction coefficient for T3A and T3B ERCOFTAC cases [18]. Results from the new model, from the WC formulation [1] and obtained using AGS criterion [10] – with a mixing length turbulence model – are plotted and compared to experimental measurements. As expected, the calculation with AGS criterion predicts too short a transition region since no parameters control turbulent production. The same trend can be observed in the case of WC formulation. On the contrary, considering the T3B

case, both WC and AGS predict too late a transition onset. The behaviour of the new model corresponds well to the measurements taking into account both the transition onset and the extent of the transition zone.

4.2. Influence of the free-stream turbulence length scale

The influence of the turbulence length scale Le on the model was then analysed using the Jonáš *et al.* experimental results [22]:

$$Le = -\frac{\left(\overline{u'^2}\right)_e^{3/2}}{\overline{U}_e \frac{\partial\left(\overline{u'^2}\right)_e}{\partial x}}, \tag{29}$$

These cases all occur at the same zero-pressure-gradient free-stream velocity of 5 m/s, with the same FST level of 3% at the leading edge but with different turbulence integral length scales. The turbulence integral length scale characterises the turbulence spectrum shape and thus influences the turbulence decay (*i.e.* the local amplitude of the TKE) as well as the receptivity process.

The shape factor evolution for 3 cases from Jonáš *et al.* is plotted in Fig. 9. Only the results from 3 of the 6 Jonáš *et al.* cases are displayed in the graph, since the results obtained for the other cases have comparable features.

For $Le = 0.038$ m (Fig. 9 (a)), both the AGS criterion and the WC model do not enable to predict a transition onset. It provides instead a fully laminar boundary-layer flow with a constant shape factor value $H_{12} = 2.59$. Only the new model predict a transition onset. Transition position prediction is well reproduced by the new model around $Re_x = 200000$. Moreover, the new model is the only one that takes into account the influence of the streaks on the mean flow in the laminar zone for this case. The distortion of the laminar flow by the streaks leads to a slight decrease of the shape factor. Nonetheless, the new model underpredicts the extent of transitional zone compared to measurements. Numerically, the transition takes place between $200000 < Re_x < 300000$ while experimentally it extends from 20000 to 500000. The comparison between the $Le = 0.153$ m (b) and $Le = 0.333$ m (c) cases shows a good behaviour on the new model's part when the turbulence integral length varies. The influence of

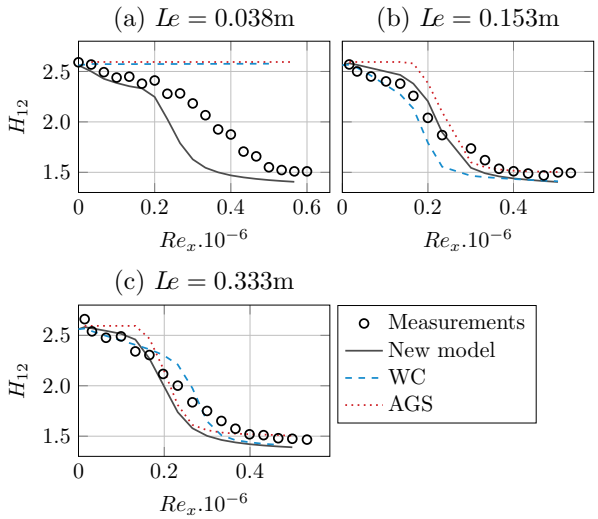

Figure 9: Shape factor evolution for 3 of the 6 cases from Jonáš *et al.* (symbols) ($Tu_0 = 3\%$ with different integral length scales Le), calculated with the current model (New model, plain line), the Walters & Cokljat model (WC, dashed line) and the Abu-Ghannam and Shaw criterion (AGS, dotted line).

the streaks on the laminar flow, as well as the transition onset and the extent of the transitional region are well represented by the new model compared to the measurements. On the contrary, the WC model shows a non-physical behaviour, since the transition onset is predicted sooner in the case of $Le = 0.153$ m (b), with a lower local Tu than in the case of $Le = 0.333$ m (c). The AGS criterion detects also accurately the transition position in both cases, but it does not enable to take into account a streak influence on the mean flow.

4.3. Influence of the pressure gradient

The influence of the pressure gradient is analysed with the help of ERCOFTAC T3C cases: T3C1, T3C2, T3C3 and T3C5. The T3C4 case has not been taken into account because it presents a flow separation, and because the model cannot simulate laminar separation bubbles. The skin friction coefficients for these cases are depicted in Fig. 10; all four are subjected to the same pressure gradient (with different free-stream velocities), displayed in Fig. 11. The tran-

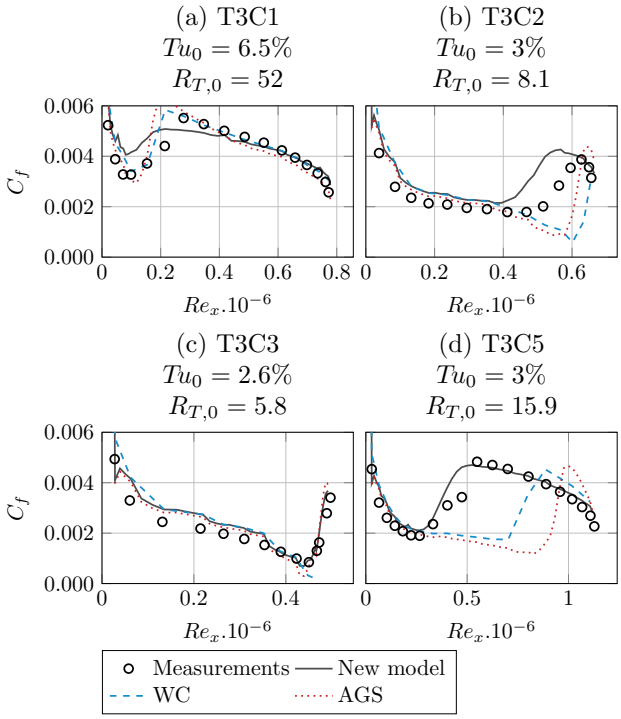

Figure 10: Streamwise evolution of the skin friction coefficient for the ERCOFTAC T3C1 (a), T3C2 (b), T3C3 (c) and T3C5 (d) cases (symbols), calculated with the new model (plain line), the Walters & Cokljat model (WC, dashed line) and the Abu-Ghannam and Shaw criterion (AGS, dotted line).

sition onset in the T3C1 case is well calculated by the three formulations, but the extent of the transition region is underestimated each time. The new model predicts too strong a skin friction coefficient in the laminar and the transitional regions. Since the turbulence level is high in this case – $Tu_0 = 6.5\%$ at the leading edge – the transition happens close to the leading edge. For this reason, the influence of the pressure gradient is not significant in this case, compared to the three other configurations. The skin friction coefficient decreases more rapidly at the end of the plate – around $Re_x > 700000$ – due to the pressure gradient. This behaviour is well-predicted by the turbulence models used.

The AGS criterion and the WC formulation show similar features when applied to the T3C2 and to the T3C5 configurations. In both case they predict too late and too abrupt a transition, while the new model predicts more accurately the transition position and the transition extent. In the T3C2 case the transition is predicted slightly too early but the transition extent is well reproduced. It is interesting to note that these two configurations have the same turbulence level at the leading edge, but a different integral turbulence length scale and a different initial free-stream velocity. The WC formulation predicts the transition onset at approximately the same streamwise Reynolds number in both cases – around $Re_x = 600000$ in the T3C2 case and $Re_x = 700000$ in the T3C5 case. The AGS criterion predicts a later transition in the T3C5 case – around $Re_x = 850000$ – than in the T3C2 case – around $Re_x = 600000$, while the local turbulence level is more elevated in the T3C5 case, see Appendix B.

The WC formulation does not predict a transition in the T3C3 case, while both the AGS criterion and the model model predict the transition position accurately. This configuration has an initial turbulence level and a integral turbulence length scale comparable to the ones in the Jonáš *et al.* case with $Le = 0.038$ m. Since the WC formulation does not predict a transition in the $Le = 0.038$ m case, it is not surprising that it does not predict one for this configuration.

The new model accurately predicts the transition onset for these adverse-pressure-gradient cases. The extent of the transition region has however been systemat-

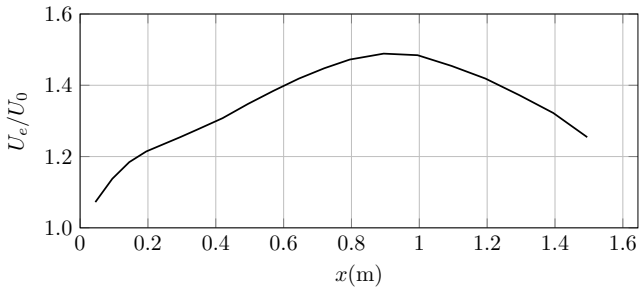

Figure 11: Streamwise evolution of the free-stream velocity divided by the leading-edge velocity, $U_e(x)/U_0$, for the T3C cases [18].

ically slightly underestimated.

5. Discussion

5.1. Behaviour of the model into the laminar boundary layer

For several reasons, the turbulent equations for k_T and ω cannot be accurate in the laminar boundary layer. Firstly, in this region, k_T is mainly dissipated by the boundary layer shear, and slowly decreases. The direct application of a turbulence model would let k_T grow. Moreover, the equation for ω is not exact and its modelling relies on a fully developed turbulence assumption, which is false as far as the laminar boundary layer is concerned.

Walters & Cokljat suggest, as a solution, to dampen the k_T production in the laminar boundary layer with a numerical intermittency, f_{INT}, which is based on the ratio between k_T and $k_T + k_L$:

$$f_{INT} = \min\left(1, \frac{k_T}{C_{INT}\left(k_T + k_L\right)}\right). \tag{30}$$

This function equals 1 whenever $k_L = 0$ and decreases whenever the ratio between k_L and k_T increases. A non-physical behaviour then appears when this solution is applied to "low"-*Tu* bypass cases, when the turbulence intensity is close to 1% at the transition onset. In these cases, a smaller FST level induces a smaller k_L-growth, and thus a higher f_{INT} function in the early laminar

boundary layer. As a consequence, turbulent kinetic energy rises – as it is not dampened – and the transition criterion is verified too early. This effect finally leads to an early transition onset, as presented in section 4, Fig. 9.

In order to solve this problem, an improvement may be suggested. In the laminar boundary layer, the TKE dissipation is mainly controlled by the near-wall dissipation. The turbulent production term was rewritten in this region to equilibrate the isotropic dissipation, $P_{k_T} = k_T\omega$. The TKE transport equation is thus reduced to the near-wall dissipation and the diffusion in the laminar zone.

5.2. Behaviour of the model in the transition region

5.2.1. Transition onset identification

Consistency with the literature review. The new criterion can be compared to the criterion originally proposed by Mayle & Schultz [36] (with u_τ as the friction velocity):

$$\frac{\max\limits_{\forall y}\left(\sqrt{\overline{u'^2}}\right)}{u_\tau} \simeq 3 \text{ at the transition onset.} \tag{31}$$

This can also be written in the following form:

$$\frac{\max\limits_{\forall y}\left(k_L\right)}{\nu \left.\frac{\partial U}{\partial y}\right|_{wall}} \simeq 4.5. \tag{32}$$

The main difference between both formulations is that Mayle & Schultz used the maximum of the k_L profile and compared it to the shear at the wall, while in the present formulation k_L is compared to the local shear in the wall-normal direction (see criterion (10)).

Analytical validation. It is valuable, for modelling purposes, to have an estimation of the streamwise Reynolds number $Re_{x,c}$ where the criterion is verified. An analysis was carried out in order to have an approximate value of this critical Reynolds number $Re_{x,c}$. The methodology is described in Appendix C. As a result of this analysis, an estimation of the critical Reynolds number can be expressed as:

$$Re_{x,c} \propto Tu_0^{-4/3}. \tag{33}$$

Figure 12 enables to compare this transitional Reynolds number $Re_{x,c}$ (Eq. 33) with experimental results gathered by Moore & Moore [43] and Abu-Ghannam & Shaw [10]. It is also compared to three transition criteria:

- the AGS criterion [10] (dashed line);
- the Mayle criterion [9] (dotted line), in which the Reynolds number based on the momentum thickness at the transition onset is expressed as a function of the initial turbulence level:

$$Re_{\theta,c} = 400 Tu_0^{-5/8}. \tag{34}$$

  In the case of a Blasius boundary layer, it can be written:

$$Re_{x,c} = 3.63 \times 10^5 Tu_0^{-5/4}; \tag{35}$$

- the Andersson *et al.* criterion [5] (loosely dashed line), based on optimal disturbances theory computations:

$$\sqrt{Re_{x,c}} Tu_0 \sim 1.2 \times 10^3. \tag{36}$$

The dispersion of the experimental data is mainly attributed to the turbulence integral scale, which is not available in most of these cases and was consequently not taken into account in this analysis. This figure also shows that the direct proportionality between the transitional Reynolds number and the upstream turbulence level raised to the power of $-4/3$ reveals a satisfactory behaviour. This proportionality corresponds to a strongly simplified version of the coupling between the k_L-equation and the transition-onset criterion, as explained in Appendix C. This result is thus considered as a partial validation of the transition criterion.

The AGS criterion shows a satisfactory behaviour if the initial turbulence level inferior to $Tu_0 \sim 7\%$. For higher turbulence level the transitional Reynolds number predicted by AGS criterion tends towards a constant value, while experimentally it continues to decrease.

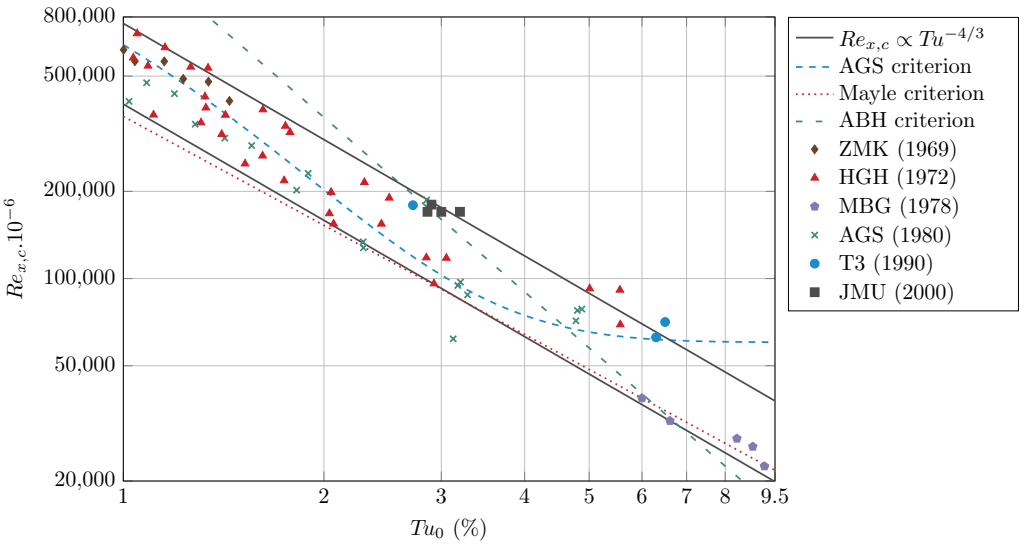

Figure 12: Transition-onset streamwise Reynolds number $Re_{x,c}$ as a function of the inflow turbulence level in a logarithmic scale graph. The curves depict the law $Re_{x,c} \propto Tu^{-4/3}$ (plain lines), the Abu-Ghannam & Shaw criterion [10] (dashed line), the Mayle criterion [9] (dotted line) and the Andersson, Berggren and Henningson (ABH) criterion [5] (loosely dashed line). The symbols represent experimental measurements from ZMK: Zysina-Molozhen & Kuznetsova [44], HGH: Hall & Hislop [45], Hislop [46] and Hall & Gibbings [47], MBG: Martin, Brown & Garrett [48], AGS: Abu-Ghannam & Shaw [10], T3: ERCOFTAC T3 [18] and JMU: Jonáš *et al.* [22].

The Mayle criterion predicts the minimum possible transitional Reynolds number for a given initial turbulence level. Its behaviour is very close to the inferior plain line, corresponding to $Re_{x,c} = 400000Tu^{-4/3}$.
The Andersson *et al.* criterion overestimates the transitional Reynolds number in cases with an initial turbulence level inferior to $Tu_0 \sim 3\%$.

5.2.2. Turbulent kinetic energy growth

In WC model, the k_T production is defined as:

$$P_{k_T} = f_\nu C_\mu f_{INT} f_W^2 \sqrt{f_{SS}} \frac{k_T S^2}{\omega}, \tag{37}$$

with f_{SS} defined as:

$$f_{SS} = \exp\left[- \left(\frac{C_{SS}\nu\Omega}{k_T} \right)^2 \right]. \tag{38}$$

In the transition region the following hypotheses can be formulated:

- the criterion is verified, then $k_T / (\nu\Omega) > 1.2$ and k_T rises because of the transfer, consequently $f_{SS} \sim 1$;
- near the wall, $f_\nu \sim \sqrt{R_T} f_W / A_\nu$;
- in the laminar boundary layer $S/\omega \sim 10^2$, thus $C_\mu \sim \omega / (A_S S)$.

The k_T production used in WC model can be approximated in the transition region by:

$$P_{k_T} \sim \frac{f_{INT} \left(C_\lambda d\right)^2 S}{A_\nu A_S} \sqrt{R_T} \omega^2. \tag{39}$$

On the one hand, the role played by ω in this production induces a shorter transition in cases presenting a higher turbulence dissipation rate. On the other hand, experiments (Jonáš *et al.* [22]) exhibit a wider transition region for higher dissipation rates. As a result, the production term had to be modified.

To improve this behaviour, two modifications are suggested in the P_{k_T} formulation:

- the multiplication by the damping function f_{tr}, to delay the growth of k_T during the transition (and thus to reproduce the transition length);

- the modification of the wall function f_W so that the turbulent production is not proportional to ω^2.

The new wall function is written f_p and is defined as:

$$f_p = \max\left(f_W, 1 - 0.7\exp\left(-\sqrt{\frac{Re_y}{37}}\right)\right), \quad \text{with } Re_y = \frac{y\sqrt{k_T}}{\nu}. \tag{40}$$

The modified P_{k_T} is defined as:

$$P_{k_T} = f_{tr} f_\nu C_\mu f_p^2 \frac{k_T}{\omega} S^2. \tag{41}$$

5.2.3. Transition dynamic control

The transition dynamic is managed by the equilibrium between the transfer term T_k, the k_T production term P_{k_T} and the k_L production term P_{k_L}. Figure 13 (a) displays contours of these three terms calculated for the ERCOFTAC T3A case, each divided by their maximum. The evolution of the wall-normal maxima of f_{tr} and β_{BP} as functions of Re_x is displayed in the same case above the contour graph, Fig. 13 (b). The k_L production is strong in the leading edge region and progressively decreases in the laminar region as the turbulent kinetic energy and the shear decrease. Once the transition has begun – indicated by the f_{tr} growth -, T_k grows and P_{k_L} tends towards zero. The transfer T_k finally decreases as k_L vanishes and the turbulent production P_{k_T} reaches its turbulent equilibrium level.

5.3. Behaviour of the model in the turbulent boundary layer

The production term of k_L is proportional to $\alpha\sqrt{k_L k_T}$, which means that a turbulent energy increase would enhance the production of k_L. This behaviour is not consistent with the dynamic of the Klebanoff modes observed in the transitional and fully turbulent regions, where they tend to disappear. In order to solve this issue, the production term of k_L has to be dampened once the transition has been activated. It cannot be set to zero, because k_L would suddenly drop and the transfer from k_L to k_T would be interrupted. This would also imply a sudden break in the k_T growth and consequently in the transition process,

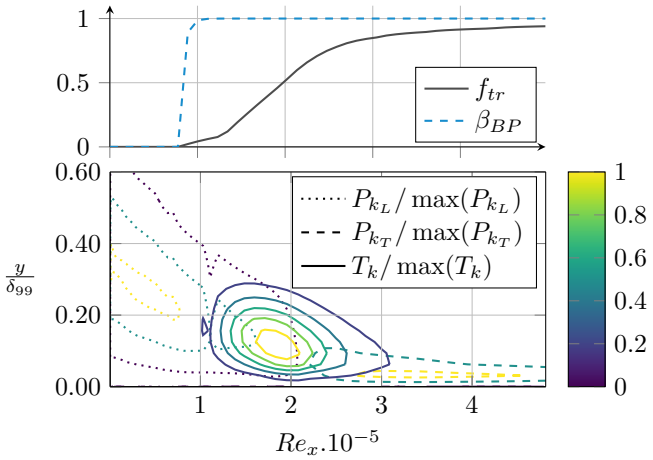

Figure 13: Above: evolution of f_{tr} and β_{BP} as functions of Re_x, calculated for the ERCOFTAC T3A case. Below: the two production terms, P_{k_T} and P_{k_L}, and the transfer term, T_k, divided each by their maximum, for the same case, given in a $(Re_x, y/\delta_{99})$ field. The abscissas are identical for the two graphs.

which would be an undesirable outcome.

One possible solution may be to dampen the k_L production thanks to the following progressive function:

$$P_{k_L} \propto \max\left(0, 1 - 1.1 f_{tr}\right), \tag{42}$$

so that P_{k_L} vanishes totally when f_{tr} approaches 1, contrary to the WC model which let k_L exist in a thin layer in the proximity of the wall.

6. Conclusion and perspectives

The accurate prediction of laminar-to-turbulent transition in Reynolds-Averaged Navier-Stokes (RANS) simulations is of substantial interest both for research and industrial purposes. Therefore, this paper describes the formulation of a physics-based bypass-transition model. The said model strongly depends on the bypass-transition physics. It is based on the Klebanoff-mode amplification, which is represented by an additional transported variable – the laminar kinetic energy (LKE). It was validated on academic configurations and gave very

promising results. It demonstrated an accurate dependence on the turbulence intensity of the external flow, on its turbulent length scale and on the free-stream pressure gradient.

Future work will first consist in validating this model by confronting it to more complex turbomachinery configurations. Then, in the present formulation, a limit was identified concerning the Reynolds stress in the transition region. This region links the laminar zone, where the anisotropy of the Reynolds stress is well-modelled, to the turbulent zone, where the Reynolds stress is represented by the Boussinesq hypothesis and is not representative of the turbulence anisotropy. To overtake this discrepancy, one could use an anisotropic turbulence modelling – following Lardeau's 2004 model [37] – combined to the new LKE approach.

Acknowledgements

This work has been founded by Safran group.

Appendix A. Influence of the $P_{\omega,3}$ term

The WC model has been studied in a fully turbulent boundary layer, in order to analyse the influence of the $P_{\omega,3}$ term – from the equation for ω – on the logarithmic law. The method implemented consists in writing the equations of the model with the following non-dimensional variables:

$$\begin{aligned} u_\tau = \sqrt{\tfrac{\tau_p}{\rho}}, \quad y^+ = \tfrac{y u_\tau}{\nu}, \quad u^+ = \tfrac{U}{u_\tau}, \\ \nu_T^+ = \tfrac{\nu_T}{\nu}, \quad k^+ = \tfrac{k}{u_\tau^2}, \quad \omega^+ = \tfrac{\nu\omega}{u_\tau^2}. \end{aligned} \tag{A.1}$$

The following hypotheses are formulated:

- the mean flow is a two-dimensional incompressible boundary layer;
- the convection terms are neglected compared to the diffusion terms.

The mean-flow equation thus becomes, with the zero-velocity condition at the wall:

$$\frac{\partial u^+}{\partial y^+} = 1 + \overline{uv}^+. \tag{A.2}$$

The velocity u^+ is thus calculated with ν_t^+, since the model rests on the Boussinesq hypothesis:

$$\overline{uv}^+ = -\nu_t^+ \frac{\partial u^+}{\partial y^+} \quad \Rightarrow \quad \frac{\partial u^+}{\partial y^+}\left(1+\nu_t^+\right) = 1. \tag{A.3}$$

The equations for the turbulence are integrated starting from the wall to a point situated in the logarithmic region. The boundary conditions at the wall are the following – $u^+ = 0$, $k_T^+ = 0$, $k_L^+ = 0$ and $\frac{\partial \omega^+}{\partial y^+} = 0$. The upper boundary conditions are the theoretical values in the logarithmic region, $k_L^+ = 0$, $k_T^+ = C_{\mu,std}^{-1/2}$ and $\omega^+ = C_{\mu,std}^{1/2}/\left(\kappa y^+\right)$. Other upper boundary conditions were tested and had no impact on the results. No condition is needed for u^+, as it is calculated with ν_t^+ and Eq. A.3.

The u^+ profile obtained with the application on the WC formulation is depicted in Fig. A.1.

The velocity profile calculated with WC formulation is bent and moves away

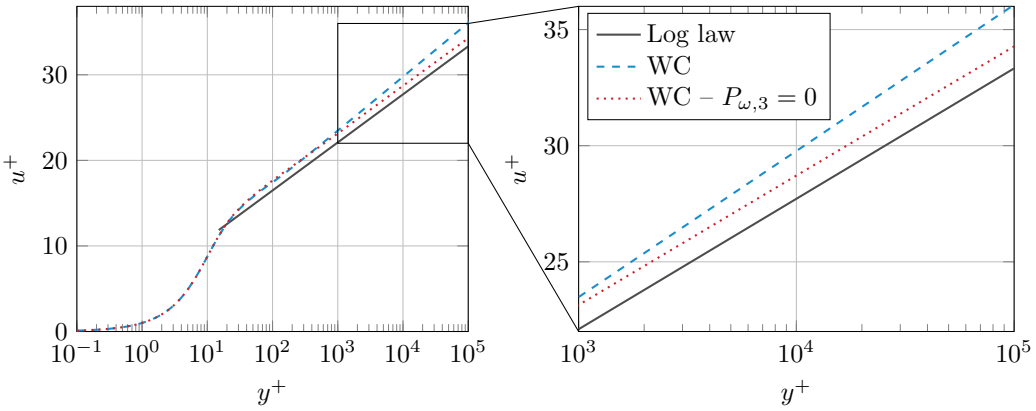

Figure A.1: Velocity profile u^+ as a function of y^+ for WC formulation in a fully turbulent boundary layer.

from the theoretical logarithmic law as y^+ increases. Nonetheless, the deletion of the term $P_{\omega,3}$ from the equation for ω has the effect to make the slope of the logarithmic law constant. Since this term deteriorates the results in the logarithmic region, the usefulness of this term was examined.

The utility of term $P_{\omega,3}$ in the WC formulation was found in its influence on the $f_{\tau,l}$ function, as Fig. A.2 illustrates. This figure depicts four functions of the WC model, which were calculated in a fully turbulent boundary layer by WC classical formulation (plain lines) and after the deletion of the term $P_{\omega,3}$ (dashed and dotted lines). The said term is used to make the behaviour of the function $f_{\tau,l}$ more abrupt, in order to dampen the production of k_L more efficiently in the turbulent region. It has thus a beneficial influence in the WC formulation.

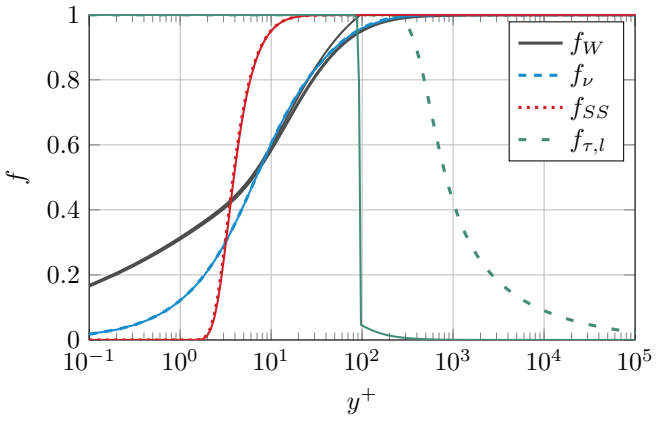

Figure A.2: Influence of the deletion of the $P_{\omega,3}$ term on the functions of the WC model. These functions are plotted as functions of y^+ in a fully turbulent boundary layer, calculated by WC formulation (plain lines) and after the deletion of the $P_{\omega,3}$ term (dashed and dotted lines).

Since the function $f_{\tau,l}$ is not used in the new formulation and since the term $P_{\omega,3}$ damages the velocity profile in the logarithmic region, this term is not used anymore.

Appendix B. Numerical parameters used to simulate academic test cases

The turbulent inflow values $k_{T,0}$ and ω_0 are determined for each test case in order to fit the measured external turbulence decay. Tab. B.2 and B.3 indicate

the Tu_0 and $\mu_{T,0}/\mu$ parameters for respectively the ERCOFTAC T3 [18] and Jonáš *et al.* [22] cases, with the following relations:

$$k_{T,0} = \frac{3}{2}\left(U_0 Tu_0\right)^2 \quad \text{and} \quad \mu_{T,0} = \rho_0 C_{\mu,std}\frac{k_{T,0}}{\omega_0}. \tag{B.1}$$

The calculated turbulence levels are plotted in Fig. B.3 and B.4 and are compared to the measurements.

Cas	U_0 (m/s)	Tu_0 (%)	$\frac{\mu_{T,0}}{\mu}$
T3A	5.4	3.4	12.1
T3B	9.4	6.3	99.1
T3C1	5.9	6.5	52.1
T3C2	5.0	2.9	8.1
T3C3	3.7	2.6	5.8
T3C4	1.2	2.7	2.4
T3C5	8.4	2.7	15.9

Table B.2: Numerical parameters for the ERCOFTAC T3 cases.

Cas	U_0 (m/s)	Tu_0 (%)	$\frac{\mu_{T,0}}{\mu}$
$Le = 0.022$ m	5.0	3.0	2.5
$Le = 0.038$ m	5.0	3.0	5.0
$Le = 0.059$ m	5.0	3.0	9.0
$Le = 0.153$ m	5.0	2.9	17.8
$Le = 0.159$ m	5.0	2.9	17.0
$Le = 0.333$ m	5.0	3.0	40.0

Table B.3: Numerical parameters for the Jonáš *et al.* cases.

Appendix C. Criterion consistency

The analysis presented in this appendix was carried out in order to get an approximate value of the critical Reynolds number $Re_{x,c}$ at the transition

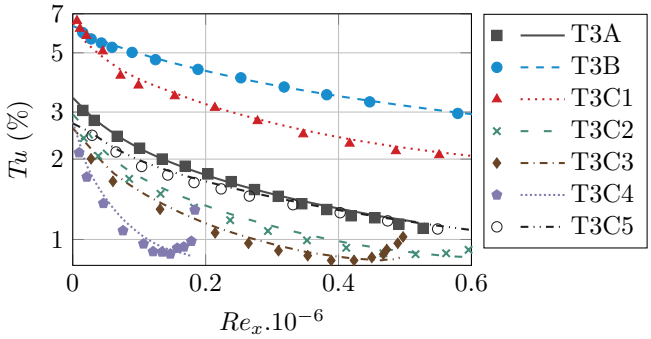

Figure B.3: External turbulence level Tu measured (symbols) on the ERCOFTAC T3 cases and calculated with the numerical parameters from Tab. B.2 (lines).

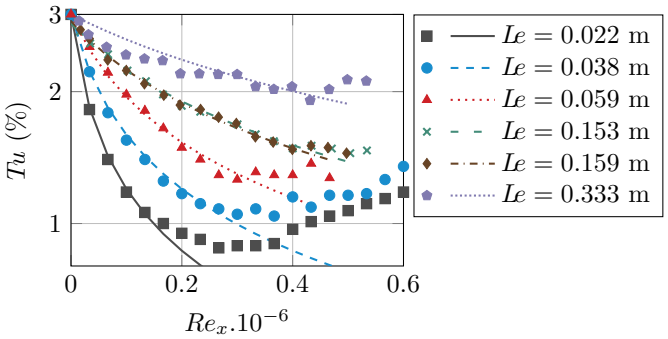

Figure B.4: External turbulence level Tu measured (symbols) on the Jonáš *et al.* cases and calculated with the numerical parameters from Tab. B.3 (lines).

location, as a function of the inflow turbulence level. Several hypotheses were applied for demonstration purpose.

1. The first hypothesis consists in neglecting the dissipation and diffusion terms in the k_L transport equation (Eq. 5). It is also assumed that the streamlines are parallel to the wall so that Eq. 5 takes the following simplified form:
$$U\frac{\partial k_L}{\partial x} = \alpha\sqrt{k_L k_T}\frac{\partial U}{\partial y}. \tag{C.1}$$
2. The second step consists in writing $U(\eta)$ for a laminar boundary layer, with $\eta = d\sqrt{U_e/(2\nu x)}$. A zero-pressure-gradient flow was considered, involving a Blasius velocity profiles (the Blasius function is denoted by $f'(\eta) = U/U_e$).
3. Another hypothesis can be applied at this stage. k_T is considered constant in the laminar boundary layer. Even if this is a very strong hypothesis, the local value of $k_T/k_{T,0}$ mainly depends on the isotropic dissipation of k_T (the ω value) and the influence of the wall. The wall effect is considered constant along x and the ω-dissipation can be taken into account – it implies to find a third-order polynomial roots – but is of no use in the context of the current analysis. Following this hypothesis, k_L takes the simple form:
$$k_L(x,\eta) = \gamma(\eta)^2 x, \quad \gamma(\eta) = \alpha\sqrt{k_T}\frac{f''(\eta)\sqrt{U_e}}{f'(\eta)\sqrt{2\nu}}. \tag{C.2}$$
4. The transition criterion will be fulfilled when $\max_\eta\left(\frac{k_L}{\nu\frac{\partial U}{\partial y}}\right) = C_{onset}$, which can be written:
$$Re_{x,c}^{\frac{3}{2}} = \max_\eta\left(\frac{2\sqrt{2}f'(\eta)^2}{3f''(\eta)}\right)\frac{C_{onset}}{(\alpha Tu_0)^2}, \tag{C.3}$$
and consequently, along x:
$$Re_{x,c} \propto Tu_0^{-\frac{4}{3}}. \tag{C.4}$$

As a result, an estimation of the critical Reynolds number can be expressed as proportional to the turbulence level Tu_0, raised to the power of $-4/3$.

References

[1] D. K. Walters, D. Cokljat, A three-equation eddy-viscosity model for Reynolds-Averaged Navier–Stokes simulations of transitional flow, Journal of Fluids Engineering 130. doi:10.1115/1.2979230.

[2] M. V. Morkovin, E. Reshotko, T. Herbert, Transition in open flow systems - a reassessment, Bulletin of the American Physical Society 39 (9).

[3] J. L. van Ingen, A suggested semi-empirical method for the calculation of the boundary layer transition region, Report VTH-74, Univ. of Techn., Dept. of Aero. Eng., Delft.

[4] A. M. O. Smith, N. Gamberoni, Transition, pressure gradient and stability theory, Douglas Aircraft Co., Report ES 26388.

[5] P. Andersson, M. Berggren, D. S. Henningson, Optimal disturbances and bypass transition in boundary layers, Physics of Fluids 11 (1) (1999) 134–150. doi:10.1063/1.869908.

[6] P. Luchini, Reynolds-number-independent instability of the boundary layer over a flat surface: optimal perturbations, Journal of Fluid Mechanics 404 (2000) 289–309. doi:10.1017/S0022112099007259.

[7] S. Zuccher, A. Tumin, E. Reshotko, Optimal disturbances in compressible boundary layers–complete energy norm analysis, AIAA Paper 5314. doi:10.2514/6.2005-5314.

[8] J. M. Lucas, Spatial optimal perturbations for transient growth analysis in three-dimensional boundary layers, Ph.D. thesis, ISAE (2014).

[9] R. E. Mayle, The role of laminar-turbulent transition in gas turbine engines, in: International Gas Turbine and Aeroengine Congress and Exhibition, Vol. 5, 1991. doi:10.1115/91-GT-261.

[10] B. J. Abu-Ghannam, R. Shaw, Natural transition of boundary layers - the effects of turbulence, pressure gradient, and flow history, Journal of Mechanical Engineering Science 22 (5) (1980) 213–228. doi:10.1243/JMES_JOUR_1980_022_043_02.

[11] P. A. Durbin, Perspectives on the phenomenology and modeling of boundary layer transition, Flow, Turbulence and Combustion 99 (2017) 1–23. doi:10.1007/s10494-017-9819-9.

[12] F. R. Menter, R. B. Langtry, S. R. Likki, Y. B. Suzen, P. G. Huang, S. Völker, A correlation-based transition model using local variables - Part I: model formulation, Journal of turbomachinery 128 (3) (2006) 413–422. doi:10.1115/1.2184352.

[13] K. J. A. Westin, R. A. W. M. Henkes, Application of turbulence models to bypass transition, Journal of fluids engineering 119 (4) (1997) 859–866. doi:10.1115/1.2819509.

[14] A. M. Savill, One-point closures applied to transition, in: Turbulence and transition modelling, 1996, pp. 233–268. doi:10.1007/978-94-015-8666-5_6.

[15] S. J. Kline, W. C. Reynolds, F. A. Schraub, P. W. Runstadler, The structure of turbulent boundary layers, Journal of Fluid Mechanics 30 (4) (1967) 741–773. doi:10.1017/S0022112067001740.

[16] P. S. Klebanoff, Effect of free-stream turbulence on a laminar boundary layer, in: Bulletin of the American Physical Society, Vol. 16, 1971.

[17] J. M. Kendall, Experimental study of disturbances produced in a pretransitional laminar boundary layer by weak freestream turbulence, in: AIAA, 18th Fluid Dynamics and Plasmadynamics and Lasers Conference, 1985.

[18] P. E. Roach, D. H. Brierley, The influence of a turbulent free-stream on zero pressure gradient transitional boundary layer development. Part I: Test

cases T3A and T3B, Numerical simulation of unsteady flows and transition to turbulence (1992) 319–347.

[19] K. J. A. Westin, B. G. Boiko, B. G. B. Klingmann, V. V. Kozlov, P. H. Alfredsson, Experiments in a boundary layer subjected to free stream turbulence. Part 1. Boundary layer structure and receptivity, Journal of Fluid Mechanics 281 (1994) 193–218. doi:10.1017/S0022112094003083.

[20] P. H. Alfredsson, M. Matsubara, Streaky structures in transition, Transitional boundary layers in Aeronautics 46 (1996) 373–386.

[21] M. Matsubara, P. H. Alfredsson, Disturbance growth in boundary layers subjected to free-stream turbulence, Journal of Fluid Mechanics 430 (2001) 149–168. doi:10.1017/S0022112000002810.

[22] P. Jonáš, O. Mazur, V. Uruba, On the receptivity of the by-pass transition to the length scale of the outer stream turbulence, European Journal of Mechanics B/Fluids 19 (5) (2000) 707–722. doi:10.1016/S0997-7546(00)01094-3.

[23] P. Andersson, L. Brandt, A. Bottaro, D. S. Henningson, On the breakdown of boundary layer streaks, Journal of Fluid Mechanics 428 (2001) 29–60. doi:10.1016/j.ijheatmasstransfer.2015.05.040.

[24] R. G. Jacobs, P. A. Durbin, Simulations of bypass transition, Journal of Fluid Mechanics 428 (2001) 185–212. doi:10.1017/S0022112000002469.

[25] L. Brandt, H. C. De Lange, Streak interactions and breakdown in boundary layer flows, Physics of Fluids 20 (2). doi:10.1063/1.2838594.

[26] M. J. P. Hack, T. A. Zaki, Streak instabilities in boundary layers beneath free-stream turbulence, Journal of Fluid Mechanics 741 (2014) 280–315. doi:10.1017/jfm.2013.677.

[27] J. G. Moore, Streaky turbulence growth before Tollmien-Schlichting waves in transition, in: 47th AIAA Fluid Dynamics Conference, no. 4418, 2017. doi:10.2514/6.2017-4418.

[28] R. Bose, P. A. Durbin, Helical modes in boundary layer transition, Physical Review Fluids 1 (7). doi:10.1103/PhysRevFluids.1.073602.

[29] M. T. Landahl, A note on an algebraic instability of inviscid parallel shear flows, Journal of Fluid Mechanics 98 (02) (1980) 243–251. doi:10.1017/S0022112080000122.

[30] A. M. Savill, New strategies in modelling by-pass transition, Closure strategies for turbulent and transitional flows 18 (2002) 492–521.

[31] T. A. Zaki, From streaks to spots and on to turbulence: Exploring the dynamics of boundary layer transition, Flow Turbulence Combustion 91 (3) (2013) 451–473. doi:10.1007/s10494-013-9502-8.

[32] P. R. Voke, Z. Yang, Numerical study of bypass transition, Physics of Fluids 7 (9) (1995) 2256–2264. doi:10.1063/1.868473.

[33] R. J. Volino, A new model for free-stream turbulence effects on boundary layers, in: International Gas Turbine and Aeroengine Congress and Exhibition, 1997. doi:10.1115/97-GT-122.

[34] D. Biau, D. Arnal, O. Vermeersch, A transition prediction model for boundary layers subjected to free-stream turbulence, Aerospace Science and Technology 11 (5) (2007) 370–375. doi:10.1016/j.ast.2006.08.011.

[35] O. Vermeersch, D. Arnal, Klebanoff-mode modeling and bypass-transition prediction, AIAA Journal 48 (11) (2010) 2491–2500. doi:10.2514/1.J050002.

[36] R. E. Mayle, A. Schulz, The path to predicting bypass transition, Journal of Turbomachinery 119 (3) (1997) 405–411.

[37] S. Lardeau, M. A. Leschziner, N. Li, Modelling bypass transition with low-Reynolds-number non-linear eddy-viscosity closure, Flow, Turbulence and Combustion 73 (1) (2004) 49–76. doi:10.1023/B:APPL.0000044367.24861.b7.

[38] D. K. Walters, J. H. Leylek, A new model for boundary layer transition using a single-point RANS approach, Journal of Turbomachinery 126 (1) (2004) 193–202. doi:10.1115/1.1622709.

[39] A. Sveningsson, Towards an extension of the $v^2 - f$ model for transitional flows, Tech. rep., Department of Thermo and Fluid Dynamics, Chalmers University of Technology (2006).

[40] M. Lopez, D. K. Walters, Prediction of transitional and fully turbulent flow using an alternative to the laminar kinetic energy approach, Journal of Turbulence (2015) 1–21doi:10.1080/14685248.2015.1062509.

[41] T. H. Shih, W. W. Liou, A. Shabbir, Z. Yang, J. Zhu, A new $k - \epsilon$ eddy viscosity model for high Reynolds number turbulent flows, Computers & Fluids 24 (3) (1995) 227–238. doi:10.1016/0045-7930(94)00032-T.

[42] W. P. Jones, B. E. Launder, Some properties of sink-flow turbulent boundary layers, Journal of Fluid Mechanics 56 (2) (1972) 337–351. doi:10.1017/S0022112072002903.

[43] J. G. Moore, J. Moore, Functional Reynolds Stress Modeling, Pocahontas Press, 2006.

[44] L. M. Zysina-Molozhen, V. M. Kuznetsova, Investigation of transition conditions in a boundary layer, Teploenergetika 16 (7) (1969) 16–20.

[45] A. A. Hall, G. S. Hislop, Experiments on the transition of the laminar boundary layer on a flat plate, no. 1843, HM Stationery Office, 1938.

[46] G. S. Hislop, The transition of a laminar boundary layer in a wind tunnel, Ph.D. thesis (1940).

[47] D. J. Hall, J. C. Gibbings, Influence of stream turbulence and pressure gradient upon boundary layer transition, Journal of Mechanical Engineering Science 14 (2) (1972) 134–146.

[48] B. W. Martin, A. Brown, S. E. Garrett, Heat transfer to a PVD rotor blade at high subsonic passage throat Mach numbers, Proceedings of the Institution of Mechanical Engineers 192 (1) (1978) 225–235.